Study of Threshold Anomaly in $^{14}N+^{56}Fe$

K. K. Jena[1,2], S. Senapati[2], P. Raj Preethi[3], P. Prema[3], S. K. Agarwalla[2]*

[1]*P. G. Department of Physics, Bhadrak Autonomous College, Bhadrak-756100, India*
[2]*P. G. Department of Applied Physics and Ballistics, Fakir Mohan University, Balasore-756019, India*
[3]*Department of Sciences, Amrita Vishwa Vidyapeetham, Ettimadai, Coimbatore-641105, India*
** Email : san1612@rediffmail.com*

Scattering of a target nucleus by another projectile nucleus is a significant way of exploring most of the nuclear properties. Experimental results can be analysed by different models of macro- and microscopic nature with optical models. We use an optical potential constructed in the light of a potential developed by Ginocchio to study elastic angular distributions of the systems $^{14}N+^{56}Fe$ near the Coulomb barrier. Our theoretical calculations match with experimental data for energies ranging from 22.4 MeV to 32.0 MeV in centre-of-mass frame. Further the potential explains the phenomenon of threshold anomaly for the system. In the present calculations our effective potential is given by

$$V_{effective}(r) = V_{Coulomb}(r) + V_{nuclear}(r) + V_{centrifugal}(r)$$

The real part $V_n(r)$ of the complex nuclear potential by putting $\lambda=1$ in the Ginocchio potential [1] assumes the form [2]

$$V_n(r) = \begin{cases} -\frac{V_B}{B_1}[B_0 + (B_1 - B_0)(1 - y_1{}^2)], 0 < r < R_0 \\ -\frac{V_B}{B_2}[B_2(1 - y_2{}^2)], \qquad r \geq R_0 \end{cases}$$

Here, $y_1 = \tanh \rho_1$, $y_2 = \tanh \rho_2$, $\rho_n=(r - R_0)b_n$ and slope parameter $b_n = \frac{\sqrt{2mV_B}}{\hbar^2 B_n}$, n = 1, 2.

The depth of potential in MeV is given by V_B at $r = R_0$. The depth of potential is controlled by B_0 at r = 0. Parameter B_n and V_B control the slope parameter b_n on either side of R_0. The inbuilt deformation in the real part of nuclear potential at $r = R_0$ shows non-trivial behaviour there. The two parts of the potential corresponding to interior (volume) region with slope b_1 and outer (surface) region with different slope b_2 are connected together to satisfy analytic continuity at $r = R_0$. This new feature invoked in the potential plays a significant role to suitably fit the experimental data of differential scattering cross-sections over a wide range of energies for the system considered here. The real part of the potential $V_n(r)$ with energy E_{CM} = 25.6 MeV is shown in Fig.1. The *non-trivial feature* is indicated by an arrow.

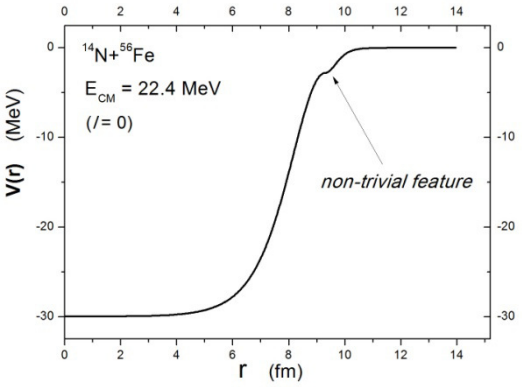

Fig.1 : Real part $V_n(r)$ of the optical potential at incident energy E_{CM} = 22.4 MeV

The imaginary part $W_n(r)$ of the new optical potential has the similar form as that of real part.

$$W_n(r) = \begin{cases} -V_{01W}\left[W_0 + \frac{W_1 - W_0}{\cosh^2\rho_1}\right], 0 < r < R_{0W} \\ -V_{02W}\left[\frac{W_2}{\cosh^2\rho_2}\right], \qquad r \geq R_{0W} \end{cases}$$

Neglecting the centrifugal term, the analyse of elastic scattering of ^{14}N ions by ^{56}Fe target deals in ten parameters out of which six parameters remain energy independent while fitting the calculated angular elastic scattering cross-sections with the experimentally measured values obtained from Ref. [3]. The independent parameters are found to remain unaltered at R_0=9.3, R_{0W}=9.4, B_1=4.4, W_0=3.0, W_1=1.1 and

W_2=0.3. The other four parameters V_B, V_{BW}, B_0 and B_2 vary with incident energies. The Coulomb radius parameter is taken to be r_c=1.25 fm. The matching is depicted individually in Fig.3. Our theoretical calculations almost agree with the experimental data which is understood from the plot depicted in Fig.2 for incident energy E_{CM} = 25.6 MeV. The values of energy-dependent parameters are taken as V_B= 3.8 MeV, V_{BW} = 1.2 MeV, B_0 = 26.99 MeV and B_2 = 0.27 for the said incident energy.

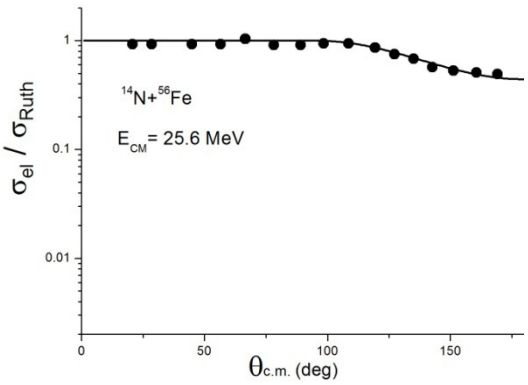

Fig.2 : Angular variation of elastic scattering cross-section of the system $^{14}N+^{56}Fe$ at incident energy E_{CM} = 25.6 MeV. Theoretically calculated results are represented by the solid curve and the experimental values taken from the Ref. [3] are represented by solid dots.

While best-fitting the theoretical data with the experimental results, we find variations in real parts and imaginary parts. Such variations are described in Fig.3.

We find the rise in magnitude of imaginary part (V_{BW}) of the optical potential with incident energy above the top of the Coulomb barrier and then saturation at a constant value of 1.4 MeV at higher energies. The variation is further accompanied by the rapid rise of real part from 2.8 MeV to 3.8 MeV near the Coulomb barrier and then fall from the top of the barrier until its strength assumes almost constant value of 2.1 MeV at higher energies. The dash-line with small stars represents the variation of real parts with energy, whereas, the dash-line with solid dots represents the simultaneous variation of imaginary parts.

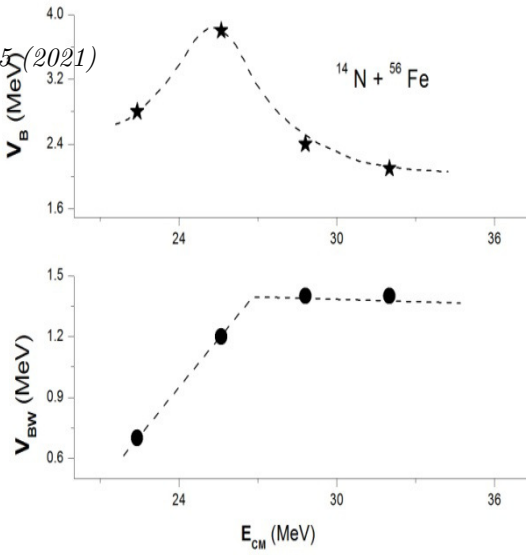

Fig.3 : Variations in real part and imaginary part of the optical potential showing the phenomenon of threshold anomaly

The bell-shape and L-shape trends in theoretical variations as shown by dash-lines for the real and imaginary parts respectively indicate the presence of *threshold anomaly* in the elastic scatterings of the system.

References

[1] J. N. Ginocchio, Ann. Phys 152,203 (1984)
[2] B. Sahu, G. S. Mallick and S. K. Agarwalla, Nucl. Phys. A 727, 299 (2003)
[3] M. E. Williams et al., Phys.Rev.C11(1975) 3